ACS OMEGA

http://pubs.acs.org/journal/acsodf

Article

New Highly Charged Iron(III) Metal−Organic Cube Stabilized by a Bulky Amine

Carlos Cruz, Andrés Igor Vega Carvallo, Evgenia Spodine, Albert Escuer, José F. Marco, Nieves Menéndez, Diego Venegas-Yazigi, and Verónica Paredes-García*

Cite This: *ACS Omega* 2020, 5, 22238−22247

Read Online

ACCESS | Metrics & More | Article Recommendations | Supporting Information

ABSTRACT: In this work, we report a new octanuclear cluster based on Fe^{III} and the ligand 1*H*-imidazole-4,5-dicarboxylic acid, $[Et_3NH]_{12}[Fe_8(IDC)_{12}]\cdot 10DMF\cdot 13H_2O$ (**1**), with a metal core containing eight Fe^{III} connected by only one type of organic ligand. A peak at 573 m/z in the mass spectra of the compound suggests the adduct species $\{[Fe_8(IDC)_{12}]+8H\}^{4-}$. By X-ray photoelectron spectroscopy, the oxidation state of the iron cation was confirmed to be 3+, also identifying the presence of a quaternary nitrogen species, which act as a countercation of the anionic metal core $[Fe_8(IDC)_{12}]^{12-}$. Mössbauer spectra recorded at different temperatures show an isomer shift and quadrupole splitting parameters that confirm the existence of only Fe^{III}-HS in the structure of **1**. X-ray analysis reveals that compound **1** crystallizes in the orthorhombic system space group *Ibam*, confirming a molecular cluster structure with an almost regular cube as geometry, with the Fe^{III} atoms located at the corners of the cube and connected by μ-1κ^2N,O:2κ^2N',O'''-IDC^{3-} bridges. Additionally, the magnetic measurements reveal a weak antiferromagnetic coupling in the Fe_8^{III} coordination cluster ($J = -3.8$ cm^{-1}). To the best of our knowledge, **1** is the first member of the family of cubes assembled with 1*H*-imidazole-4,5-dicarboxylic acid and Fe^{III} cation, exhibiting high pH stability over a broad pH range, making it an ideal candidate for the design of supramolecular structures and metal−organic frameworks.

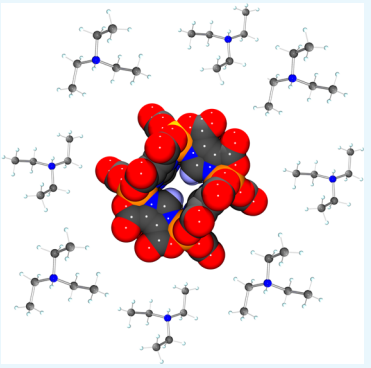

1. INTRODUCTION

One of the fascinating fields in coordination chemistry is the research in polynuclear molecular compounds, also called coordination clusters. This type of compound corresponds to molecular entities formed by multiple metal cation arrangements, connected by organic or inorganic ligands.[1] The molecular structure and properties of the coordination cluster are intrinsically related to the nature of the chosen metal center and the interaction between them through the bridging ligands.[2−4] Then, coordination clusters presenting cations with unpaired electrons are attractive in the field of molecular magnetism.[5−8] The slow relaxation of the magnetization reported for the disc-shaped $Mn_{12}^{II/III}$ compound, $[Mn_{12}O_{12}(O_2CR)_{16}(H_2O)_4]$ (R = methyl, phenyl), is a product of the high-spin state and magnetic anisotropy of the paramagnetic centers.[9,10] Furthermore, two Cr_{10}^{III} wheels bridged by acetate and alkoxide ligands, $[Cr_{10}(O_2CMe)_{10}(OR)_{20}]$, show a different magnetic behavior depending on the alkoxide ligand present in the wheel. The authors report that the methoxide ligand favors a ferromagnetic behavior, while the ethoxide ligand favors an antiferromagnetic behavior.[11] Additionally, two mixed-valence coordination clusters $[Mn_{12}^{III}Mn_7^{II}O_8(HL)_{12}(N_3)_3(MeO)_{5.5}(MeOH)_{3.5}(H_2O)_{1.5}(OH)_{0.5}](OAc)\cdot 10H_2O$ and $[Na_2Mn_{11}^{III}Mn_4^{II}O_8(HL)_{10}(OAc)_2(H_2O)_2(OCH_3)_{1.5}(N_3)_{2.5}](OAc)\cdot 10H_2O\cdot 2MeOH$ (H_3L = 2,6-(hydroxymethyl)phenol), reported in the literature exhibit the magnetocaloric effect at low temperatures due to the large spin, small anisotropy, and high density of low-lying excited states.[12] Research in coordination clusters based on Fe^{III} is interesting in molecular magnetism not only by its rich coordination chemistry but also because this spin carrier can present spin values ranging from 5/2 to 1/2, depending on the coordination environment. These features make these types of compounds attractive for applications like spin switches and magnetic refrigerants.[13−16]

From a structural viewpoint, the literature reports several Fe^{III} coordination clusters with a wide variety of nuclearities, topologies, and geometries, such as $[Fe_6(O_2)O_2(O_2CPh)_{12}(H_2O)_2]$ reported by McCusker et al.[17] and $\{[Fe_8(O)_2(OH)_{12}(tacn)_6]Br_7(H_2O)\}Br\cdot 8H_2O$ reported by Wieghardt et al.[18] (O_2CPh^- = benzoate; tacn = 1,4,7-triazacyclononane). Both compounds present planar moieties as central cores, constructed by oxides/peroxides anions in the case of Fe_6 and oxides/hydroxides anions in Fe_8. Using phosphonic acids, Konar et al. obtained $[Fe_9(\mu_3\text{-}O)_4(O_3PPh-$

Received: May 22, 2020
Accepted: July 7, 2020
Published: August 14, 2020

$(Me)_2)_3(O_2CCMe_3)_{13}]$ and $[Fe_{12}(\mu_2\text{-}O)_4(\mu_3\text{-}O)_4(O_2CCHPh_2)_{14}(4\text{-}^t buPhPO_3H)_6]$ ($O_3PPh(Me)_2^{2-}$ = 3,5-dimethylphenyl phosphonate; $O_2CCMe_3^-$ = pivalate; $O_2CCHPh_2^-$ = diphenylacetate; $4\text{-}^t buPhPO_3H^-$ = *p*-^{t}butylphenyl phosphonate), with Fe_9 and Fe_{12} central cores, showing an icosahedral and a double butterfly structure, respectively.[19] Kang et al. reported the mixed-valence $Fe_{18}^{III}Fe_{24}^{II}$ coordination cluster $[\{Fe(Tp)(CN)_3\}_{24}\{Fe(H_2O)_2\}_6\{Fe(dpp)(H_2O)\}_{12}(CF_3SO_3)_6]\cdot 18H_2O$ (Tp = hydrotris(pyrazolyl)borate; dpp = 1,3-di(4-pyridyl)propane).[20] The $Fe_{18}^{III}Fe_{24}^{II}$ cluster has a number large enough of metal centers to be considered as a nanocage.[20]

From the experimental viewpoint, several polynuclear Fe^{III} compounds found in the literature were synthesized using two or more ligands, giving rise in many cases to complex structures.[21−23] In this article, we report a novel Fe_8^{III} octanuclear cube-type coordination cluster $[Et_3NH]_{12}[Fe_8(IDC)_{12}]\cdot 10DMF\cdot 13H_2O$ (**1**) obtained using 1*H*-imidazole-4,5-dicarboxylic acid (H_3IDC) as a unique ligand. The structure and composition of the octanuclear cluster were obtained by single-crystal X-ray diffraction, X-ray photoelectron spectroscopy (XPS), and other complementary techniques. Furthermore, the characterization of **1** was complemented with Mössbauer spectroscopy, electronic paramagnetic resonance, and magnetic susceptibility measurements.

2. EXPERIMENTAL SECTION

2.1. Synthesis of $[Et_3NH]_{12}[Fe_8(IDC)_{12}]\cdot 10DMF\cdot 13H_2O$ (1). Caution: The reaction involves the mixture of a moderate amount of triethylamine (Et_3N) and glacial acetic acid (CH_3COOH). Fuming vapors are released, so care must be taken in this procedure.

To a suspension of $Fe(acac)_3$ (0.5 mmol) and H_3IDC (1 mmol) in a mixture of 10 mL of water and *N*,*N*′-dimethylformamide (DMF) (1:1 H_2O/DMF), 5 mL of Et_3N was added with constant stirring. After a few minutes, the suspension disappears, and the resulting dissolution changes the initial orange color to a deep red color. After 10 min of stirring, 5 mL of glacial CH_3COOH was added, giving a deep reddish-brown solution, which was left undisturbed for a few weeks, giving yellow prismatic crystals of **1** (Figure S1). MW = 4475.86 g/mol. Yield: 50% based on iron(III) salt. Anal. Calc. for: $C_{162}H_{300}N_{46}O_{71}Fe_8$ (**1**): C, 43.47%; H, 6.77%; N, 14.40%; Fe, 9.98%. Found: C, 43.35%; H, 6.71%; N, 14.36%; Fe, 9.98%.

2.2. Physical Measurements. *2.2.1. Elemental Analysis.* The quantitative content of C, H, and N was obtained on a Thermos CHNS flash 2000 elemental analyzer using solid crystalline samples of **1**. The quantitative content of Fe was determined using atomic absorption spectroscopy. Three samples of **1** from different batches were measured in triplicate. Solid crystalline samples of **1** were digested in a 0.5% HNO_3 solution, and the iron concentration was measured with a Perkin Elmer PinAAcle 900F atomic absorption spectrophotometer equipped with an acetylene burner using a flux of acetylene:air of 2.51:10 L min^{-1} as an oxidant mixture. An Fe lamp of 248.33 nm wavelength was used with standard solutions in a linear range of 0.1−3,0 mg_{Fe} L^{-1}.

2.2.2. Mass Spectrometry. Mass spectra were measured in a Linear Ion Trap LTQ-XL Thermo Scientific spectrometer and were analyzed with the software MMass 5.5.0.[24−26] The analysis was carried out in a DMF:H_2O solution of **1** (pH ≈ 6.0) in negative ion mode, scanning in a range of m/z of 150−1500 (Table S2 shows the peak list of the mass spectrum).

2.2.3. Thermogravimetric Analysis. Thermogravimetric (TG) analysis was performed on a Mettler Toledo TGA/DSC STAR system. The samples were introduced in an alumina holder and heated under a nitrogen atmosphere from room temperature to 900 °C at a heating rate of 5 °C/min.

2.2.4. Single-Crystal X-ray Diffraction. A single crystal of **1** was directly selected from the reaction beaker and glued on the tip of a capillary glass using epoxy resin. Scans on the Bruker APEXII diffractometer confirmed enough crystal quality to perform full recording using X-ray radiation of Mo Kα (λ = 0.71073 Å). The data were reduced by SAINT,[27] and empirical absorption corrections were applied using SADABS.[28] The structure was solved with the ShelXT[29] structure solution program using direct methods and refined with the ShelXL[30] refinement package with least-squares minimization. Additional data concerning the crystallographic and the refinement parameters are detailed in the Supporting Information. TopOsPro 5.0 software[31] was used for structure drawing. During the structure completion process by difference Fourier synthesis, it was clear that there was a high amount of space left by the Fe_8 cubes of the complex within the cell, having an ill-defined electron density. Although the triethylammonium and water molecules were identified preliminarily at this point, refinement by any model we tried was unsuccessful. Efforts to measure at low temperatures failed since crystals crack. Synthetic modifications were also tried to change triethylammonium by an alkaline metal or other ammonium such as tetramethylammonium or tetraethylammonium without any good results. Since efforts to model the disorder of the solvating molecules by using a meaningful scheme failed, a well-documented method for the modeling of unresolved electron density, PLATON-SQUEEZE, was used.[32,33] Alert B is present in the check cif file. CHEMS01 Type_1 is due to the use of the "$[Fe_8C_{60}H_{12}N_{24}O_{48}$ + solvent]" expression to remark that the reported formula $Fe_8C_{60}H_{12}N_{24}O_{48}$ lacks a specific amount of solvent and countercations molecules because of the use of SQUEEZE. PLAT084 and PLAT230 can be assigned to the unresolved effects such as the disorder in chemical species. Despite this, most of the structural determination alerts are related to cation/solvent disorder, thus allowing one to consider that the geometry for the Fe_8 cluster is reliable. Therefore, based on the complementary analyses, 12 triethylammonium (Et_3NH^+) as counterions, 10 *N*,*N*′-dimethylformamide, and 13 water crystallization molecules per Fe_8 cube unit were included in the final formula ($C_{162}H_{300}N_{46}O_{71}Fe_8$).

2.2.5. X-ray Photoelectron Spectroscopy. XPS data were recorded using a PHOIBOS-150 hemispherical electron analyzer (Specs) under a pressure lower than 2×10^{-9} mbar using Al Kα radiation. The X-ray gun was operated at a power of 100 W to minimize radiation-induced damage to the sample. All the spectra were recorded at a constant pass energy of 30 eV. The binding energy scale was referenced to the main C 1s contribution due to aliphatic carbon, which was set at 284.6 eV. All spectra were computer-fitted to a sum of pseudo-Voigt profiles using Shirley background subtraction.

2.2.6. Mössbauer Spectroscopy. The Mössbauer spectra of finely ground crystals of **1** were recorded between 295 and 4.2 K. The measurements were recorded using two $^{57}Co(Rh)$ γ-ray sources mounted on both ends of an electromagnetic transducer operated in the triangular mode. One of the sources was used for energy calibration with α-Fe (6 μm) foil. The spectra were analyzed by a nonlinear fit using the NORMOS program,[34] and the energy calibration was made using α-Fe (6 μm) foil. Variable

https://dx.doi.org/10.1021/acsomega.0c02420
ACS Omega 2020, 5, 22238−22247

temperatures were obtained with an Oxford Spectromag 4000 M cryostat connected to an ITC-503 Oxford Instruments temperature controller. To avoid saturation effects and optimize the signal-to-noise ratio, the sample thickness was 10 mg of natural Fe cm^{-2}.

2.2.7. Electronic Paramagnetic Resonance. EPR spectra were collected on a Bruker EMX-1572 spectrometer working at 9.39 GHz (X-band) using polycrystalline samples of **1** at 298 K.

2.2.8. Magnetic Measurements. Magnetic measurements were carried out using a Quantum Design Dynacool Physical Properties Measurement System (PPMS) equipped with a vibrating sample magnetometer (VSM). The dc data were collected under externally applied fields of 1 kOe in the 1.8−300 K temperature range. Also, magnetization measurements at the variable field were performed at 1.8, 3, 5, and 8 K from 0 to 90 kOe. The magnetic signal from the sample holder was negligible to affect our data accuracy and was not considered. Diamagnetic corrections (estimated from Pascal constants) were considered.[35] The simulation of the temperature-dependent magnetic susceptibility data was performed by exact diagonalization of the spin Hamiltonian employing the PHI software.[36]

3. RESULTS AND DISCUSSION

3.1. Synthesis. Concerning the synthesis of **1**, the organic ligand H_3IDC can be considered as a polyprotic acid. Depending on the pH of the media, this ligand can be present in the final product with different protonation degrees (Scheme 1).

Scheme 1. pK_a Values of the Organic Ligand H_3IDC

$$H_3IDC \leftrightharpoons H_2IDC^- + H^+ \quad pKa_1 = 5.3$$
$$H_2IDC^- \leftrightharpoons HIDC^{2-} + H^+ \quad pKa_2 = 8.2$$
$$HIDC^{2-} \leftrightharpoons IDC^{3-} + H^+ \quad pKa_3 = 11.8$$

The initial suspension of H_3IDC in an H_2O/DMF mixture gave a pH near 3, indicating that the full protonated H_3IDC should be the predominant species in this media. When triethylamine (Et_3N; 36 mmol) was added, the pH increased to 11, causing a displacement of the equilibrium to the more reactive ionic species $HIDC^{2-}/IDC^{3-}$, which are now able to coordinate the Fe^{III} centers. Then, at the end of the reaction, the acidification with glacial acetic acid (87 mmol) decreased the pH of the solution to 4. Regarding the pH fluctuation in the reaction and the different protonation degrees of the H_3IDC ligand ($IDC^{3-}/HIDC^{2-}/H_2IDC^-$), it is possible to infer that the assembly of iron(III) with the organic species should generate multiple possibilities for the final formula of Fe_8^{III} cluster. Thus, an anionic $[Fe_8(IDC)_{12}]^{12-}$, neutral $[Fe_8(HIDC)_{12}]$, or cationic $[Fe_8(H_2IDC)_{12}]^{12+}$ species could be considered as a product. Considering that the species of the ligand are dependent on the pH, it is reasonable to infer that IDC^{3-} anion should be the predominant species at pH = 11 (pK_{a3} = 11.8), being also able to coordinate the Fe^{III} cations to give the Fe_8 cluster $[Fe_8(IDC)_{12}]^{12-}$. Later, the pH decreases to 4, causing the quantitative protonation of Et_3N (pK_a = 10.8) needed to induce the crystallization of the anionic cluster, $[Fe_8(IDC)_{12}]^{12-}$. The fact that the Fe_8 cluster was assembled under a basic medium and crystallized under a acidic medium can be taken as evidence about the chemical stability of $[Fe_8(IDC)_{12}]^{12-}$ over a broad pH range.

Figure S2 shows the mass spectrum of **1** obtained by the linear ion trap in the range of 150−1500 *m*/*z*. The base peak at 573 *m*/*z* correlates very well with the adduct species $\{[Fe_8(IDC)_{12}]+8H\}^{4-}$. Other adducts species with lower intensities were also identified at 1147, 764, and 458 *m*/*z*, which correlate with $\{[Fe_8(IDC)_{12}]+10H\}^{2-}$, $\{[Fe_8(IDC)_{12}]+9H\}^{3-}$, and $\{[Fe_8(IDC)_{12}]+7H\}^{5-}$, respectively. This result corroborates that the anionic species $[Fe_8(IDC)_{12}]^{12-}$ is the correct representation for the Fe_8 cluster.[37,38]

3.2. X-ray Single-Crystal Structural Characterization. X-ray single-crystal analysis reveals that **1** corresponds to a discreet octanuclear cluster forming a cubic polyhedron, which crystallizes in the highly symmetric *Ibam* orthorhombic system (Table 1). Each corner of the cube is occupied by one Fe^{III}

Table 1. Crystallographic Refinement Data for 1

empirical formula	$C_{162}H_{300}N_{46}O_{71}Fe_8$[a]
formula weight (g mol^{-1})	4475.86[a]
temperature (K)	293(2)
crystal system	orthorhombic
space group	*Ibam*
a (Å)	18.051(8)
b (Å)	29.079(13)
c (Å)	33.766(15)
α (°)	90
β (°)	90
γ (°)	90
volume ($Å^3$)	17,724(13)
Z	4
ρ_{calc} (g/cm^3)	0.856
μ (mm^{-1})	0.692
F(000)	4528.0
crystal size (mm^3)	0.986 × 0.363 × 0.274
radiation	Mo Kα (λ = 0.71073)
2θ range for data collection (°)	5.954−52
index ranges	$-22 \le h \le 22$, $-35 \le k \le 35$, $-41 \le l \le 41$
reflections collected	67,448
independent reflections	8864 [R_{int} = 0.0848, R_{sigma} = 0.0601]
data/restraints/parameters	8864/0/320
goodness-of-fit on F^2	1.297
final *R* indices [$I \ge 2\sigma(I)$]	*R*1 = 0.1537, w*R*2 = 0.3714
final *R* indices [all data]	*R*1 = 0.2003, w*R*2 = 0.4078
largest diff. peak/hole (e $Å^{-3}$)	2.08/−1.05

[a]The empirical formula and molecular weight given in the table consider the counterions and solvate molecules determined by all the analysis techniques used in the experimental section.

center (Figure 1a), being the edges organic ligands. Continuous shape measurement (CShM) was used to evaluate the distortion of the cube. The iron moiety was compared with an ideal cube using the SHAPE software,[39] obtaining a CShM value of 0.004 and confirming an almost perfect cubic arrangement of the coordination cluster (Table S3). This cube is obtained by the asymmetric unit containing two crystallographically independent iron centers and three full deprotonated IDC^{3-} ligands. Fe(1) and Fe(2) present the same coordination environment, FeN_3O_3, produced by the coordination of three $\kappa N,O$-IDC^{3-} molecules, which also form three independent FeNCCO chelate rings (Figure 1b). The geometry of each FeN_3O_3 moiety was also compared with an ideal octahedron using the SHAPE. CShM values of 1.13 and 1.00 were obtained for Fe(1) and Fe(2), respectively, confirming that the geometry of both cations is well described as octahedron (Tables S4 and S5). On the other hand, as depicted in Figure 1c, the IDC^{3-} anion is

https://dx.doi.org/10.1021/acsomega.0c02420
ACS Omega 2020, 5, 22238−22247

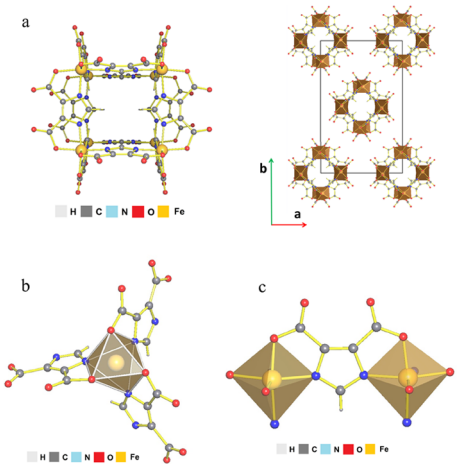

Figure 1. (a) Molecular structure of **1** and view of the packing through the *c* axis. (b) Coordination environment of Fe^{III} centers in **1** and (c) μ-1κ^2N,O:2κ^2N',O''' bis-chelating bridge mode of IDC^{3-}.

acting as the μ-1κ^2N,O:2κ^2N',O'''-IDC^{3-} bis-chelating bridge, leading to an intercation distance of Fe(1)···Fe(2) = 6.3754(3) Å (Figure 1c). Additionally, each [Fe(IDC)$_3$] moiety is chiral, being the handedness of Fe(1) Λ and Fe(2) Δ. Because of the Λ−Δ alternating arrangement, a centrosymmetric compound is obtained. In compound **1**, the Fe−N and Fe−O bond distances are in the range of 2.028(7)−2.093(7) Å and 1.985(6)−2.003(7) Å for Fe(1) and in the range of 2.069(7)−2.098 (7) Å and 1.979(7)−2.005(7) for Fe(2). Usually, in coordination compounds, the bond distance can be associated with the oxidation and spin state of the cation. For example, Angaridis et al. reported two molecular systems [Fe(3,5-^{t}Bu$_2$salpn)(MeDCBI)Fe(3,5-^{t}Bu$_2$-salpn)] and {[Fe(3,5-^{t}Bu$_2$salpn)]$_2$(HDCBI)} (3,5-^{t}Bu$_2$salpn = dianion of 1,3-bis-[(di-*tert*-butylsalicylidene)amino]propane); H_2MeDCBI = 4,5-dicarboxy-1-methyl-1*H*-imidazole; H_3DCBI = 4,5-dicarboxyimidazole).[40] Both compounds are based on Fe^{III} in a high-spin state (HS), having an FeN_3O_3 environment formed by κ^2N,O'-$HDCB^{2-}$/κ^2N,O'-$MeDCBI^{2-}$ and κ^4O,N,N',O'-3,5-^{t}Bu$_2$salpn, being the cations bridged by μ-1κ^2N,O:2κ^2N',O'''-imidazole ligand as in **1** and presenting Fe−N = 2.126(3)−2.107(1) and Fe−O = 1.883(2)Å−2.223 Å bond distances.[40] Also, in other imidazoles Fe^{III}-HS compounds, the average Fe−N is 2.091 Å.[41] All these data permitted us to infer that the Fe(1) and Fe(2) cations present in **1** can be assigned as Fe^{III}-HS. Therefore, the iron cluster previously determined from structural X-ray measurements can be represented as $[Fe_8(IDC)_{12}]^{12-}$.

Literature reports different analogous M_8-H_nIDC^{n-3} compounds based on other transition metal cations (**2**−**18**), which are summarized in Table 2. For example, Liu et al. obtained under solvothermal conditions an anionic Ni^{II} cluster, $[Ni_8(HIDC)_{12}]^{8-}$ (**2**). This Ni_8^{II} cube is surrounded by a large number of solvent molecules and protonated 4,4′-trimethylenedipiperidine as countercations.[42] Likewise, by a solvothermal reaction, Xu et al. reported the synthesis of another 0D Ni^{II}-neutral cubic cluster $[(Ni_8(H_2IDC)_8(HIDC)_4)]\cdot 8(C_2H_5OH)\cdot 18(H_2O)$ (**3**), in which the H_3IDC ligand is found both as di- and monoprotonated species and also surrounded by solvate molecules.[43] Meanwhile, Cheng et al. reported the synthesis at room temperature of another anionic cluster without solvate molecules $[Me_4N]_{20}[Co_8(IDC)_{12}]$ (**4**),[44] but unfortunately, the crystalline structure was not reported in the publication. Moreover, extended networks obtained from the M_8 anionic cluster and stabilized by the incorporation of a second metal cation have also been reported (**5**−**10**). In these cases, the imidazole ligand is present in the full deprotonated form (IDC^{3-}), giving a cluster with a highly negative charge. For compounds **6**−**10**, the anionic cluster is stabilized by the linkage of alkaline cations to the carboxylate groups belonging to the imidazole ligand.[45] Besides, Cheng et al. reported a mixed-valence Co^{II}/Co^{III} cubic cluster forming a 1D heterometallic coordination polymer $[Ni(cyclam)]_4[Ni(cyclam)(H_2O)_2]_2\{[Ni(cyclam)][Co_8(IDC)_{12}]\}\cdot 41H_2O$ (**5**). This extended compound is assembled by the $[Co_6^{II}Co_2^{III}(IDC)_{12}]^{14-}$

Table 2. Summary of M_8 Cubes Reported in the Literature

formula of the compound	synthesis type	dimension	charge of the cluster	H_3IDC species	ref
$[Et_3NH]_{12}[Fe_8(IDC)_{12}]\cdot 10DMF\cdot 13H_2O$ (**1**)	R.T.[e]	0D	−12	IDC^{3-}	this work
$Ni_8(HIDC)_{12}(H_2TMDP)_4(DMF)_4(EtOH)_4(H_2O)_6$[a] (**2**)	solvothermal	0D	−8	$HIDC^{2-}$	42
$[(Ni_8(H_2IDC)_8(HIDC)_4)]\cdot 8(C_2H_5OH)\cdot 18(H_2O)$ (**3**)	solvothermal	0D	0	$H_2IDC^-/HIDC^{2-}$	43
$[Me_4N]_{20}[Co_8(IDC)_{12}]$[b] (**4**)	R.T.	0D	−20	IDC^{3-}	44
$[Ni(cyclam)]_4[Ni(cyclam)(H_2O)_2]_2$ (**5**)	R.T.	1D	−14	IDC^{3-}	44
$\{[Ni(cyclam)][Co_8(IDC)_{12}]\}\cdot 41H_2O$[c]					
$K_{20}[Ni_8IDC_{12}]\cdot 74(H_2O)$ (**6**)	R.T.	3D	−20	IDC^{3-}	43
$K_{20}[Ni_8IDC_{12}]\cdot 50(H_2O)$ (**7**)	R.T.	3D	−20	IDC^{3-}	43
$K_{20}[Ni_8IDC_{12}]\cdot 29(H_2O)$ (**8**)	R.T.	3D	−20	IDC^{3-}	43
$\{[Li_{11}(Ni_8IDC_{12})(H_2O)_{12}]Li_9(H_2O)_{20}\}$ (**9**)	solvothermal	3D	−20	IDC^{3-}	45
$\{[Na_{20}(Ni_8IDC_{12})(H_2O)_{28}](H_2O)_{13}(CH_3OH)_2\}$ (**10**)	solvothermal	3D	−20	IDC^{3-}	45
$Zn_{12}(guanidinium)_8(IDC)_8(HIDC)_4\cdot(DMF)_8(H_2O)_3$ (**11**)	solvothermal	3D	−16	$HIDC^{2-}/IDC^{3-}$	46
$Cd_8Na_8(HIDC)_8(IDC)_4(H_2Pip)_2\cdot(EtOH)_5(H_2O)_{37}$[d] (**12**)	solvothermal	3D	−12	$HIDC^{2-}/IDC^{3-}$	46
$Zn_8K_8(HIDC)_{12}(DMF)_5(H_2O)_{16}$ (**13**)	solvothermal	3D	−8	$HIDC^{2-}$	46
$Cd_8K_8(HIDC)_{12}(DMF)_5(H_2O)_{16}$ (**14**)	solvothermal	3D	−8	$HIDC^{2-}$	46
$Co_8K_8(HIDC)_{12}(DMF)_5(H_2O)_{16}$ (**15**)	solvothermal	3D	−8	$HIDC^{2-}$	46
$Mn_8K_8(HIDC)_{12}(DMF)_5(H_2O)_{16}$ (**16**)	solvothermal	3D	−8	$HIDC^{2-}$	46
$[Cr_4In_4(HIDC)_{12}]\cdot H_2O$ (**17**)	solvothermal	0D	0	$HIDC^{2-}$	47
$[Cr_{7.28}In_{0.72}(HIDC)_{12}]\cdot H_2O$ (**18**)	solvothermal	0D	0	$HIDC^{2-}$	47

[a]H_2TMDP^{2+} = 4,4′-trimethylenedipiperidinium. [b]Me_4N^+ = tetramethylammonium, crystalline structure not reported. [c]cyclam = 1,4,8,11-tetraazacyclotetradecane. [d]H_2Pip^{2+} = piperazinium. [e]R.T. = room temperature.

https://dx.doi.org/10.1021/acsomega.0c02420
ACS Omega 2020, 5, 22238−22247

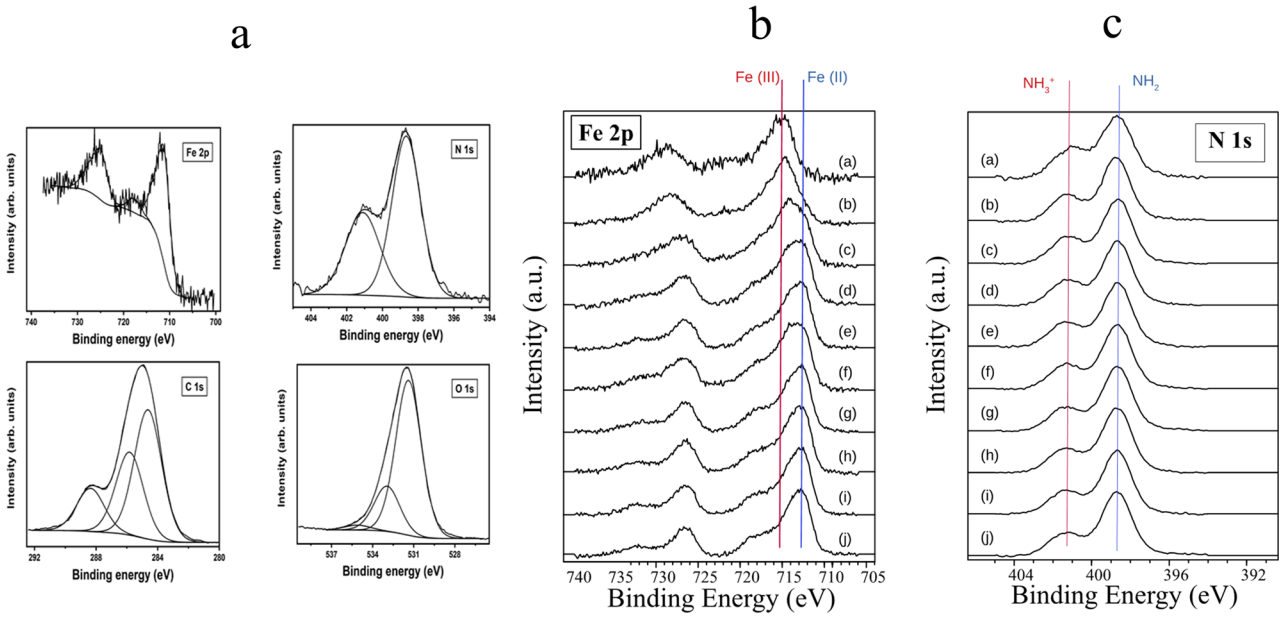

Figure 2. (a) High-resolution Fe 2p, N 1s, C 1s, and O 1s XPS spectra. (b) Fe 2p spectra recorded after different exposure times to the X-ray beam of the XPS spectrometer: (a) 7 min, (b) 42 min, (c) 107 min, (d) 172 min, (e) 237 min, (f) 302 min, (g) 367 min, (h) 432 min, (i) 497 min, and (j) 562 min. Note the progressive transformation of the initial Fe^{III}-HS species in an Fe^{II}-HS species. (c) N 1s spectra recorded after different exposure times to the X-ray beam of the XPS spectrometer: (a) 12 min, (b) 77 min, (c) 142 min, (d) 205 min, (e) 270 min, (f) 367 min, (g) 432 min, (h) 497 min, (i) 562 min, and (j) 592 min. Note how the intensity of the initial triethylammonium (Et_3NH^+) species decreases with increasing X-ray irradiation times.

cluster, which is coordinated by the carboxylate group to the $[Ni(cyclam)]^{2+}$ complexes.[44]

On the other hand, Alkordi et al. reported six 3D networks built from M_8^{II} anionic cubes (**11**−**16**).[46] $Zn_{12}(guanidinium)_8(IDC)_8(HIDC)_4{\cdot}(DMF)_8(H_2O)_3$ **11** and $Cd_8Na_8(HIDC)_8(IDC)_4(H_2Pip)_2(EtOH)_5(H_2O)_{37}$ **12** contain $HIDC^{2-}$ and IDC^{3-} species as ligands. In the case of **11**, the negative charge is balanced by both guanidinium and zinc cations, being the zinc cations also coordinating the carboxylates groups belonging to the anionic cubes originating in this form the 3D structure. For **12**, sodium and a protonated amine (piperazinium) are also balancing the charge of the cubic cluster. The authors also report a series of compounds $M_8K_8(HIDC)_{12}(DMF)_5(H_2O)_{16}$ (M = Zn^{II}, Cd^{II}, Co^{II}, and Mn^{II}) (**13**−**16**), containing only the $HIDC^{3-}$ species as a ligand, but in these cases, only alkaline cations are stabilizing the $[M_8(HIDC)_{12}]^{8-}$ cluster in the 3D networks. The two last examples (**17** and **18**) were reported by Zhai et al.[47] and correspond to In^{III}-Cr^{III} heterometallic 0D cubes $[Cr_4In_4(HIDC)_{12}]{\cdot}H_2O$ and $[Cr_{7.28}In_{0.72}(HIDC)_{12}]{\cdot}H_2O$, being neutral species and only including the $HIDC^{2-}$ in the structure.

In our case, although the molecular structure of the Fe_8^{III} core was well identified by X-ray single-crystal analysis due to the size of the cluster and the high symmetry of the cell, part of the electronic density surrounding the cluster remained invisible for this technique, as has also been reported in an analogous cobalt octanuclear cluster.[44] However, according to the examples mentioned above, the full deprotonated IDC^{3-} species generates M_8 cubes with the highest negative charge, which is stabilized by other metal cations or bulky protonated amines. Then, 12 counterions must be present in the compound to neutralize the negative charge of the resulting $[Fe_8(IDC)_{12}]^{12-}$ cluster. Since no additional iron centers were found in the intercluster space, only the triethylammonium cation should be acting as a counterion. This counterion also provides enough steric hindrance to avoid the assembly between the iron clusters, thus producing a molecular crystal packing for **1**, as was also reported for the Ni_8^{II} analogous system with 4,4′-trimethylene-dipiperidinium.[42] Accordingly, XPS, TG, and FTIR were performed to complement the structural characterization.

3.3. XPS. To gather more information about the chemical composition of **1**, Fe 2p, N 1s, C 1s, and O 1s high-resolution XPS spectra were also collected (Figure 2a). The Fe 2p spectrum consists of an asymmetric spin-orbit doublet with binding energies of the Fe $2p_{3/2}$ and Fe $2p_{1/2}$ core levels of 711.5 and 725.2 eV, respectively, and a small shake-up satellite at 717.8 eV. The shape of the spectrum, the binding energies of its different components, and the presence of the small satellite are all characteristic of iron in 3+ oxidation state and high-spin configuration,[48,49] confirming the observation in the structural characterization. The N 1s spectrum was best-fitted to two contributions. The major one, located at a binding energy of 398.7 eV, can be ascribed to an amine-type or aromatic-type N−H bond belonging to the imidazole ring of the organic ligand.[50,51] The higher binding energy component at 401.1 eV is characteristic of a quaternary nitrogen species,[50,51] which must belong to the triethylammonium (Et_3NH^+) present in the intercluster space of **1** and acting as a countercation. A fit considering also the contribution to the N 1s spectrum of a ternary amine was not successful, discarding the presence of trimethylamine in the final product. The C 1s spectrum contains three different carbon species at 284.6, 285.8, and 288.4 eV, which can be associated with C−C or C−H bonds; C−N, C−O, C═N, or C ≡ N bonds; and O—C═O bonds, respectively.[50,51] The O 1s spectrum contains three contributions. The main one at 531.4 eV can be associated with C═O bonds in O═C—O groups, while the second one at 533.0 eV may correspond to C−O bonds in O═C—O groups.[50,51] The minor component at 535.0 eV might be ascribed to a small oxygen satellite.

All the identified bonds are part of the IDC^{3-} anionic ligand present in the cluster $[Fe_8(IDC)_{12}]^{12-}$. Nevertheless, from a

https://dx.doi.org/10.1021/acsomega.0c02420
ACS Omega 2020, 5, 22238−22247

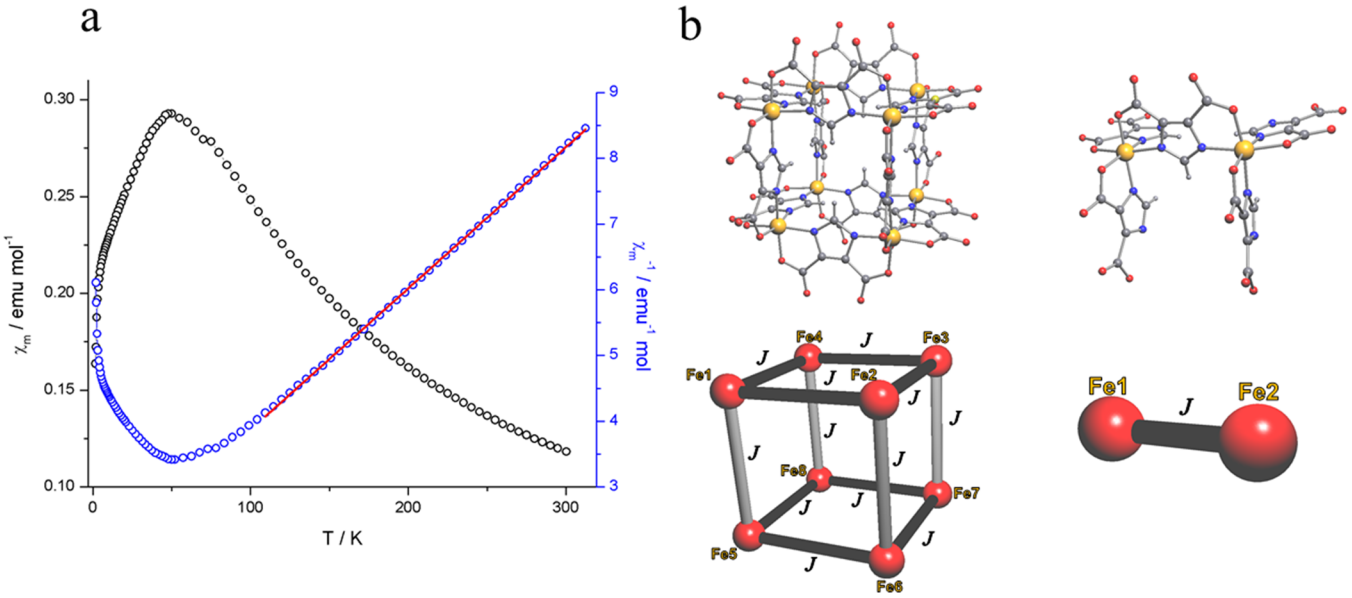

Figure 3. (a) Plots of χ_m vs T and χ_m^{-1} vs T for **1**. (b) Images of magnetic pathways for the Fe_8 moiety in **1** and the binuclear Fe_2 simplified model.

chemical viewpoint, the presence of a quaternary nitrogen species corroborates that triethylammonium (Et_3NH^+) is the countercation of the anionic iron cluster, which is also consistent with the reaction condition used to obtain **1**. Therefore, the molecular structure of the iron cluster is deduced to be $[Et_3NH]_{12}[Fe_8(IDC)_{12}]$.

An important fact that was found during the development of this work is that the sample is very sensitive to the irradiation by the X-rays of the XPS spectrometer and that it undergoes important chemical changes after relatively short irradiation times. To minimize the occurrence of these changes, we used a low power in the X-ray gun (100 W against the more usual 300 W) and slightly higher pass energy (30 eV vs the usual 20 eV) to record the data. Using a constant pass energy of 30 eV instead of 20 eV allows recording the spectra with a larger number of counts in a given time without compromising too much the energy resolution. So, for the Fe 2p spectrum shown in Figure 2b, we used only one scan (less than 5 min of irradiation) since increasing the number of scans can lead to chemical changes.Figure 2b collects the Fe 2p spectra recorded after several increasing irradiation times. It is evident that, even after short irradiation times (see spectra (b) and (c) in Figure 2b), the lines of the Fe 2p spectrum shift to lower binding energies and a strong shake-up satellite starts developing at around 714 eV. These results clearly indicate that the initial Fe^{III}-HS is progressively reduced to an Fe^{II}-HS species upon X-ray irradiation. In fact, the spectra recorded at intermediate irradiation times contain both Fe^{II}-HS/Fe^{III}-HS contributions. After long irradiation times (Figure 2b), the Fe 2p spectrum only shows the presence of Fe^{II}-HS species.[49] Important changes are also observed in the N 1s spectra 2c. In this case, a decrease in the intensity of the protonated Et_3NH^+ species is observed upon X-ray irradiation. However, and contrary to the iron case, the quaternary nitrogen species appears to be more resilient, as it is still present after long irradiation times. The mechanisms giving place to chemical changes under X-ray irradiation in XPS are complex and have been commented in detail elsewhere.[51] In particular, in the case of the reduction of metal cations in oxides, interionic Auger decay processes appear to play an important role.[50] Among all the chemical changes reported, the degradation of quaternary nitrogen species (deprotonation) has also been reported for some organic compounds.[50] The results are relevant because they stress the need of being extremely careful when recording XPS data for this type of compound. Otherwise, erroneous conclusions can be drawn from the recorded data.

3.4. FTIR and Thermogravimetric Measurements.

Figure S3a,b shows the infrared spectra of **1**, compared with those of trimethylamine in acidic media and *N*,*N*-dimethylformamide. A clear match of the first two spectra between 3000 and 2400 cm^{-1} can be observed, in agreement with the presence of the cationic Et_3NH^+ species in **1** (Figure S3a). Also, the strong absorption at 1680 cm^{-1} (observed in the spectrum of **1**) is exactly in the same position of the C═O vibration associated with DMF molecules (Figure S3b), indicating that this molecule must also be present in the final formula. Additionally, thermogravimetric analysis was performed under a nitrogen atmosphere (Figure S4) to characterize the presence of solvent molecules and thermal stability of **1**. The cluster is stable until 250 °C, showing two weight losses of 5.2% (30−90 °C) and 16.1% (190−250 °C) associated with solvate molecules. Considering that both H_2O and DMF were used as a solvent in the synthesis of **1** and as it has been reported for other compounds,[52] it is reasonable to assign the first loss to the release of 13 water molecules (5.2%) and the second one to 10 DMF molecules (16.3%). At higher temperatures, a third weight loss of 30.2% (250−360 °C) is observed. Literature data show that triethylammonium salts (triethylammonium bis-7,7,8,8-tetracyanoquinodimethane) have a thermal decomposition process between 195 and 220 °C.[53] Additionally, the inorganic cluster ($[(HTEA)(TEA)_{0.75}]_2[PSb_2^{III}Mo_5^{V}Mo_7^{VI}O_{40}]$) shows a continuous weight loss (14.6%) between 44 and 573 °C, which is attributed by the authors to the release of tryethylamine.[54] Therefore, the loss of 30.2% can be associated to the release of 12 trimethylamine (27.4%) belonging to 12 Et_3NH^+ acting as counterions.[55] Considering the solvate molecules, the final formula of **1** is $[Et_3NH]_{12}[Fe_8(IDC)_{12}]\cdot 10DMF\cdot 13H_2O$, which correlates very well with the elemental analysis given in the experimental section (section 2.1.1). With these results in mind, Mössbauer spectroscopy, electronic paramagnetic resonance,

https://dx.doi.org/10.1021/acsomega.0c02420
ACS Omega 2020, 5, 22238−22247

and magnetic susceptibility measurements were also performed to characterize the properties of $[Et_3NH]_{12}[Fe_8(IDC)_{12}]\cdot 10DMF\cdot 13H_2O$.

3.5. EPR and Magnetic Measurements. The X-band EPR spectrum at room temperature of a polycrystalline sample of **1** shows a broad signal characteristic of an Fe^{III}-HS ion with $S = 5/2$,[56,57] with a line width of 376 G and a resonant field of 3330 G giving a value of $g = 2.016$ (Figure S5a). Magnetic measurements of **1** as a function of temperature were performed using a polycrystalline sample in the range of 1.8−300 K at 1 kOe. The temperature dependence of the magnetization is shown in Figure 3a as χ_m vs T and χ_m^{-1} vs T plots. The χ_m vs T plot shows an increase in the χ_m value as the temperature is lowered, leading to a maximum of 0.3 emu mol^{-1} at 50 K. From this temperature, a constant decrease is observed, leading to a non-zero value of 0.2 emu mol^{-1} at 1.8 K. On the other hand, the χ_m^{-1} vs T plot gives C and θ values of 44.6 emu mol^{-1} and −73.2 K, respectively. Furthermore, a 35.5 emu K mol^{-1} value is obtained at room temperature (4.44 emu K mol^{-1} per Fe^{III} center) from the $\chi_m T$ vs T plot (Figure S5b), close to the expected for eight non-interacting Fe^{III}-HS centers, 35.56 emu K mol^{-1} considering $S_{Fe} = 5/2$ and $g = 2.016$. Lowering the temperature, the $\chi_m T$ product constantly decreases as the temperature reaches 100 K. Below this temperature, a more pronounced decrease is observed, reaching a minimum value of 0.3 emu K mol^{-1} at 1.8 K. Clearly, the susceptibility data shows that an antiferromagnetic behavior is the predominant phenomenon of the Fe_8^{III} coordination cluster. Field-dependent magnetization measurements were performed at 1.8, 3, 5, and 8 K and represented as N_β vs H and N_β vs HT^{-1} plots (Figure S6). The curves N_β vs H show a lack of saturation at the studied conditions, leading to a maximum near to 4 μ_B at 90 kOe, very far than the value expected for eight Fe^{III} cations in high spin (40 μ_B). For an antiferromagnetic system with a spin state of $S = 0$ at low temperatures, the observed magnetization only can belong from non-zero spin states that are close to the ground state. Then, the absence of saturation and the small values obtained for the magnetization corroborate that antiferromagnetic interactions predominate in the Fe_8^{III} coordination cluster at low temperatures.

As Figure 3 shows, 12 equivalent μ-1κ^2N,O:2κ^2N',O''' magnetic pathways can be established (the edges of the cube) between the eight Fe^{III}-HS in the octanuclear molecular structure of **1**, leading to the following spin Hamiltonian:

$$\hat{H}_8 = -JS_{Fe1}S_{Fe2} - JS_{Fe2}S_{Fe3} - JS_{Fe3}S_{Fe4} - JS_{Fe4}S_{Fe1} - JS_{Fe5}S_{Fe6} - JS_{Fe6}S_{Fe7} - JS_{Fe7}S_{Fe8} - JS_{Fe5}S_{Fe8} - JS_{Fe1}S_{Fe5} - JS_{Fe2}S_{Fe6} - JS_{Fe3}S_{Fe7} - JS_{Fe4}S_{Fe8}$$

No analytical model has been developed for such a complex system. For this reason, the use of a simplified model was necessary. Considering the symmetry of the cluster, the cubic system can be simplified to a binuclear system that consists in two Fe^{III}-HS cations, connected by a single μ-1κ^2N,O:2κ^2N',O''' bridge (Figure 3b), leading to the following spin Hamiltonian:

$$\hat{H}_2 = -JS_{Fe1}S_{Fe2}$$

A fit of the experimental susceptibility data by matrix diagonalization using the $\hat{H}_2$ spin Hamiltonian using the PHI[36] software was performed between 300 and 1.8 K, considering $S_{Fei} = 5/2$ and maintaining the g factor fixed to the experimental value obtained by EPR, $g = 2.016$ (Figure 4). A

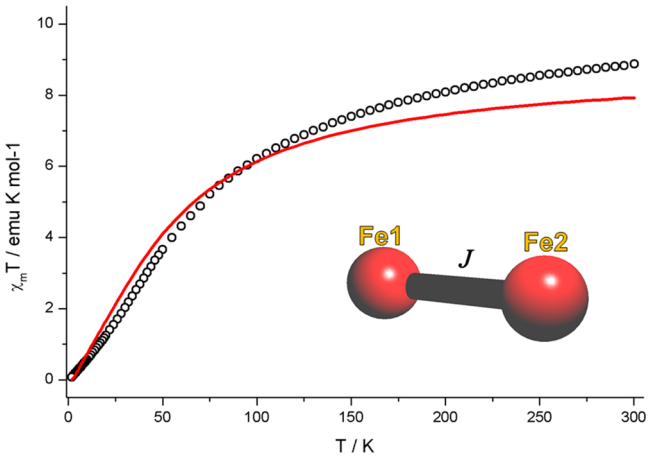

Figure 4. Fitting of $\chi_m T$ vs T at 1 kOe and using a simplified binuclear model.

magnetic coupling constant of $J = -3.8$ cm^{-1} was obtained, with an agreement factor of $R = 8.5 \times 10^{-3}$ ($R = \Sigma(\chi_m T_{obs}) - (\chi_m T_{exp})^2/\Sigma(\chi_m T_{obs})^2$). The use of a free g value gave a better fit (Figure S5c), obtaining J and g values of −5.28 cm^{-1} and 2.178, respectively. In both cases, the negative sign and a similar magnitude of the magnetic exchange coupling confirm the antiferromagnetic nature of the superexchange interaction of Fe^{III}-HS cations through μ-1κ^2N,O:2κ^2N',O''' bridges. However, the use of a g value of 2.016, obtained from EPR measurements, seems to be more adequate and in agreement with the structural features of the Fe^{III}-HS cations. The magnitude and sign of the coupling constants also are in agreement with the antiferromagnetic interactions observed by Angaridis et al.[40] between Fe^{III}-HS/Fe^{III}-HS mediated by μ-1κ^2N,O:2κ^2N',O''' bridges with $J = -4.8(2)$ cm^{-1}. The interaction between Fe^{III}-HS/Fe^{III}-HS can be rationalized considering the five magnetic orbitals associated with Fe^{III}-HS in an octahedral environment (two e_g and three t_{2g}). Thus, the interaction through the IDC^{3-} ligand generates a greater possibility of overlapping between the five orbitals of each Fe^{III}-HS center.[58] The fact that the binuclear model presents a rather moderate fit of the magnetic behavior can be explained on the base of the crude simplification of the octanuclear structure of **1**. An analogous Ni_8^{II} cluster was reported by Liu et al.,[42] $(H_2TMDP)_4(DMF)_4(EtOH)_4(H_2O)_6[Ni_8(HImDC)_{12}]$ (DMF = *N*,*N*′-dimethylformamide, EtOH = ethanol, and H_2TMDP = 4,4′-trimethylenedipiperidinium), having the same cubic structure of **1** and the same μ-1κ^2N,O:2κ^2N',O''' connectivity between the metal cations. This compound also presents an antiferromagnetic behavior, with an identical χ_m vs T tendency compared with **1**. Although no exchange coupling values were given for this Ni_8 cluster, this example suggests that the bulk magnetic properties of such cubic systems are related not only with the particular magnetic interactions of the metal cations through μ-1κ^2N,O:2κ^2N',O''' but also with the spin topology arrangement within the whole cluster structure. In any case, more experimental and theoretical analyses should be performed to clarify the magnetic behavior of compound **1**, perhaps studying the orbitals involved in each magnetic exchange pathway and the role of the topology of the cluster in the bulk magnetic properties.

3.6. Mössbauer Spectroscopy. The temperature evolution of the Mössbauer spectra of **1** at 295, 77, and 4.2 K is shown in Figure 5. In the studied temperature range, each spectrum consists of a doublet, corroborating that Fe(1) and Fe(2)

https://dx.doi.org/10.1021/acsomega.0c02420
ACS Omega 2020, 5, 22238−22247

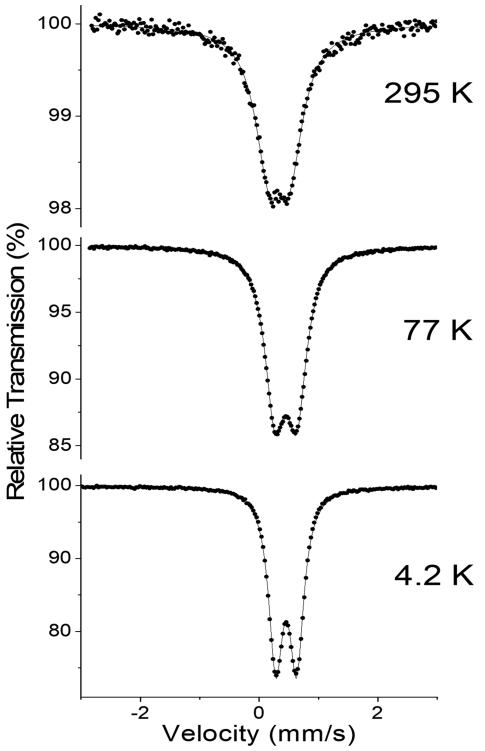

Figure 5. Mössbauer spectra of **1** at different temperatures.

present the same coordination environment. Furthermore, the Mössbauer parameters at room temperature, isomer shift (δ = 0.336(1) mm s^{-1}) and quadrupole splitting (ΔE_Q = 0.369(4) mm s^{-1}), are characteristics of Fe^{III}-HS. As the temperature decreases, the isomer shift increases, δ = 0.447(1) mm s^{-1} at 4.2 K, according to the second-order Doppler shift; nevertheless, the quadrupole splitting is nearly independent of the temperature (ΔE_Q = 0.352(2) mm s^{-1} at 4.2 K), as expected for Fe^{III}-HS ions for which the quadrupolar interaction is due only to the lattice contribution. In the same way, the presence of only a doublet even at 4.2 K would be indicative of the absence of magnetic order or that the relaxation time is shorter than the lifetime of the nuclear excited state.[59] For the antiferromagnetic Fe^{III}-HS coupled system, a sextet should be observed in the Mössbauer spectrum, below the critical temperature (50 K). Nevertheless, the spectra recorded at room temperature, 77 K, and 4 K are almost the same, consisting of a sharp doublet instead of a sextet. This behavior indicates that the relaxation time of compound **1** is shorter than the lifetime of the nuclear excited state (experimental measurement time, 10^{-7} s).[51] Such kind of paramagnetic fast spin relaxation has also been reported for other polynuclear Fe^{III}-HS coupled systems.[60,61]

4. CONCLUSIONS

A new iron octanuclear coordination cluster **1** was successfully synthesized under an acid−base reaction using a single ligand, 1*H*-imidazole-4,5-dicarboxylic acid (H_3IDC). The cluster $[Fe_8(IDC)_{12}]^{12-}$ is formed in basic media and crystallized in acid media, proving the chemical stability of the anionic Fe_8 cluster in a wide pH range. On the other hand, XPS is a very powerful technique that permitted to identify the existence of triethylammonium cations as a charge compensator that balance the charge of the anionic cluster, and to corroborate the chemical identity of the cluster $[Fe_8(IDC)_{12}]^{12-}$ determined by single-crystal X-ray diffraction. Moreover, it was possible to identify that a reduction process centered on the metal cation is produced under experimental conditions of the XPS technique. In fact, the recorded data have to be carefully analyzed to obtain the correct information on the oxidation state of the metal cation in this type of compound. Additionally, Mössbauer spectroscopy corroborated the spin and oxidation state of the iron center within the cluster, leaving no doubt that only Fe^{III}-HS ions are present in the structure of **1**. The performed magnetic measurements revealed that weak antiferromagnetic coupling is dominant in the whole temperature range. Although the literature reports the existence of Mn^{II}, Ni^{II}, $Co^{II/III}$, Zn^{II}, and Cr^{III}-In^{III} negative or neutral cubic analogous systems forming 0D, 1D, or 3D compounds with either H_2IDC^-/$HIDC^{2-}$/IDC^{3-} anionic species, compound **1** is the first member of this family based on Fe^{III}. Despite the challenges presented for the characterization of **1**, the present work collects a complete chemical and physical description of a new Fe^{III}-HS coordination cluster with a novel cubic structure.

■ ASSOCIATED CONTENT

Supporting Information

The Supporting Information is available free of charge at https://pubs.acs.org/doi/10.1021/acsomega.0c02420.

Image of the yellow prismatic crystals of **1** (Figure S1); mass spectra (Figure S2); FTIR spectra (Figure S3); TG in the N_2 atmosphere (Figure S4); EPR spectra, $\chi_m T$ vs T plot at 1 kOe; best-fit curve at 1 kOe (Figure S5); N_β vs H and N_β vs HT^{-1} plot (Figure S6); complete crystal data and structure (Table S1); peak list of mass spectra (Table S2); and results of CShM calculation (Tables S3−5) (PDF)

Crystal data and structure refinement for **1** (CIF)

■ AUTHOR INFORMATION

Corresponding Author

Verónica Paredes-García − *Facultad de Ciencias Exactas, Departamento de Ciencias Químicas, Universidad Andres Bello, 8370146 Santiago, Chile; CEDENNA, 8380494 Santiago, Chile;* orcid.org/0000-0002-7537-7430; Phone: +56-2-26615756; Email: vparedes@unab.cl

Authors

Carlos Cruz − *Facultad de Ciencias Exactas, Departamento de Ciencias Químicas, Universidad Andres Bello, 8370146 Santiago, Chile; CEDENNA, 8380494 Santiago, Chile*

Andrés Igor Vega Carvallo − *Facultad de Ciencias Exactas, Departamento de Ciencias Químicas, Universidad Andres Bello, 8370146 Santiago, Chile; CEDENNA, 8380494 Santiago, Chile;* orcid.org/0000-0001-6501-4161

Evgenia Spodine − *CEDENNA, 8380494 Santiago, Chile; Facultad de Ciencias Químicas y Farmacéuticas, Departamento de Química Inorgánica y Analítica, Universidad de Chile, 8380492 Santiago, Chile*

Albert Escuer − *Departament de Química Inorgànica, Universitat de Barcelona, 08028 Barcelona, Spain;* orcid.org/0000-0002-6274-6866

José F. Marco − *Instituto de Química Física Rocasolano, 28013 Madrid, Spain*

Nieves Menéndez − *Departamento de Química Física Aplicada, Facultad de Ciencias, Universidad Autónoma de Madrid, 28049 Madrid, Spain*

https://dx.doi.org/10.1021/acsomega.0c02420
ACS Omega 2020, 5, 22238−22247

Diego Venegas-Yazigi − *CEDENNA, 8380494 Santiago, Chile; Facultad de Química y Biología, Departamento de Química de los Materiales, Universidad de Santiago de Chile, 9170022 Santiago, Chile;* orcid.org/0000-0001-7816-2841

Complete contact information is available at: https://pubs.acs.org/10.1021/acsomega.0c02420

Notes

The authors declare no competing financial interest.

Accession code CCDC 1810846 contains the supplementary crystallographic data for this publication. These data can be obtained free of charge via www.ccdc.cam.ac.uk/data_request/cif, or by emailing data_request@ccdc.cam.ac.uk, or by contacting The Cambridge Crystallographic Data Centre, 12 Union Road, Cambridge CB2 1EZ, UK; fax: +44 1223 336033.

■ ACKNOWLEDGMENTS

The authors acknowledge FONDECYT 1170887, Proyecto Anillo CONICYT ACT 1404 grant, CONICYT-FONDEQUIP/PPMS/EQM130086, CONICYT-FONDEQUIP/EQM140060, Chilean-French International Associated Laboratory for Multifunctional Molecules, and Materials LIAM3-CNRS N°1027 for financial support. The authors also acknowledge Financiamiento Basal, AFB180001, CEDENNA and Laboratory of Analyses of Solids (L.A.S-UNAB). JFM acknowledges financial support from the Spanish Agencia Estatal de Investigación (AEI) through Project No. RTI2018-095303-B-C51 and the Comunidad de Madrid through Project. NANOMAGCOST-CM P2018/NMT-4321. NM acknowledges Agencia Estatal de Investigación Española PGC2018-095642-B-I00 proyect.

■ REFERENCES

(1) Cronin, L.; Fielden, J. *Coordination Clusters. In Encyclopedia of Supramolecular Chemistry*; 1st ed.; Atwood, J. L. Ed.; Taylor and Francis: London, Published online 2007; 1−10, DOI: 10.1081/E-ESMC-120024346.

(2) Kostakis, G. E.; Powell, A. K. An Approach to Describing the Topology of Polynuclear Clusters. *Coord. Chem. Rev.* **2009**, *253*, 2686−2697.

(3) Sivaramakrishna, A.; Clayton, H. S.; Makhubela, B. C. E.; Moss, J. R. Platinum Based Mixed-Metal Clusters (PtnMm(CO)xLy, M = Ru or Os; n + m = 2 to 10 and Ly = Other Ligands)-Synthesis, Structure, Reactivity and Applications. *Coord. Chem. Rev.* **2008**, *252*, 1460−1485.

(4) Kostakis, G. E.; Perlepes, S. P.; Blatov, V. A.; Proserpio, D. M.; Powell, A. K. High-Nuclearity Cobalt Coordination Clusters: Synthetic, Topological and Magnetic Aspects. *Coord. Chem. Rev.* **2012**, *256*, 1246−1278.

(5) Beltran, L. M. C.; Long, J. R. Directed Assembly of Metal-Cyanide Cluster Magnets. *Acc. Chem. Res.* **2005**, *38*, 325−334.

(6) Peng, J.-B.; Zhang, Q.-C.; Kong, X.-J.; Zheng, Y.-Z.; Ren, Y.-P.; Long, L.-S.; Huang, R.-B.; Zheng, L.-S.; Zheng, Z. High-Nuclearity *3d-4f* Clusters as Enhanced Magnetic Coolers and Molecular Magnets. *J. Am. Chem. Soc.* **2012**, *134*, 3314−3317.

(7) Müller, A.; Peters, F.; Pope, M. T.; Gatteschi, D. Polyoxometalates: Very Large Clusters Nanoscale Magnets. *Chem. Rev.* **1998**, *98*, 239−272.

(8) Zhang, S.; Cheng, P. Coordination-Cluster-Based Molecular Magnetic Refrigerants. *Chem. Rec.* **2016**, *16*, 2077−2126.

(9) Sessoli, R.; Tsai, H. L.; Schake, A. R.; Wang, S.; Vincent, J. B.; Folting, K.; Gatteschi, D.; Christou, G.; Hendrickson, D. N. High-Spin Molecules: $[Mn_{12}O_{12}(O_2CR)_{16}(H_2O)_4]$. *J. Am. Chem. Soc.* **1993**, *115*, 1804−1816.

(10) Sessoli, R.; Gatteschi, D.; Caneschi, A.; Novak, M. A. Magnetic Bistability in a Metal-Ion Cluster. *Nature* **1993**, *365*, 141−143.

(11) McInnes, E. J. L.; Anson, C.; Powell, A. K.; Thomson, A. J.; Poussereau, S.; Sessoli, R. Solvothermal Synthesis of $[Cr_{10}(\mu\text{-}O_2CMe)_{10}(\mu\text{-}OR)_{20}]$ 'Chromic Wheels' with Antiferromagnetic (R = Et) and Ferromagnetic (R = Me) Cr(III)···Cr(III) Interactions. *Chem. Commun.* **2001**, *10*, 89−90.

(12) Liu, J.-L.; Leng, J.-D.; Lin, Z.; Tong, M.-L. Ferromagnetic Homometallic Mn_{19} Cluster and Heterometallic Na_2Mn_{15} Cluster with Large Spin State as Magnetic Refrigerants. *Chem. − Asian J.* **2011**, *6*, 1007−1010.

(13) Goura, J.; Chandrasekhar, V. Molecular Metal Phosphonates. *Chem. Rev.* **2015**, *115*, 6854−6965.

(14) Kitashima, R.; Imatomi, S.; Yamada, M.; Matsumoto, N.; Maeda, Y. Gradual Two-step Spin Crossover Behavior of Binuclear Iron(III) Complex Bridged by *trans*-1,2-Bis(4-pyridyl)ethylene. *Chem. Lett.* **2005**, *34*, 1388−1389.

(15) Sheikh, J. A.; Jena, H. S.; Clearfield, A.; Konar, S. Phosphonate Based High Nuclearity Magnetic Cages. *Acc. Chem. Res.* **2016**, *49*, 1093−1103.

(16) Evangelisti, M.; Candini, A.; Ghirri, A.; Affronte, M.; Piligkos, S.; Brechin, E. K.; McInnes, E. J. L. Molecular Nanoclusters as Magnetic Refrigerants: The Case of Fe_{14} with Very Large Spin Ground-State. *Polyhedron* **2005**, *24*, 2573−2578.

(17) McCusker, J. K.; Christmas, C. A.; Hagen, P. M.; Chadha, R. K.; Harvey, D. F.; Hendrickson, D. N. Spin Frustration: A Hexanuclear Ferric Complex with a S = 5 Ground State. *J. Am. Chem. Soc.* **1991**, *113*, 6114−6124.

(18) Weighardt, K.; Pohl, K.; Jibril, I.; Huttner, G. Hydrolysis Products of the Monomeric Amine Complex $(C_6H_{15}N_3)FeCl_3$: The Structure of the Octameric Iron(III) Cation of $\{[(C_6H_{15}N_3)_6Fe_8(\mu_3\text{-}O)_2(\mu_2\text{-}OH)_{12}]Br_7(H_2O)\}Br{\cdot}8H_2O$. *Angew. Chem., Int. Ed. Engl.* **1984**, *23*, 77−78.

(19) Konar, S.; Clearfield, A. Synthesis and Characterization of High Nuclearity Iron(III) Phosphonate Molecular Clusters. *Inorg. Chem.* **2008**, *47*, 5573−5579.

(20) Kang, S.; Zheng, H.; Liu, T.; Hamachi, K.; Kanegawa, S.; Sugimoto, K.; Shiota, Y.; Hayami, S.; Mito, M.; Nakamura, T.; Nakano, M.; Baker, M. L.; Nojiri, H.; Yoshizawa, K.; Duan, C.; Sato, O. A Ferromagnetically Coupled Fe_{42} Cyanide-Bridged Nanocage. *Nat. Commun.* **2015**, *6*, 5955.

(21) Winpenny, R. E. P. High Nuclearity Clusters: Clusters and Aggregates with Paramagnetic Centers: Oxygen and Nitrogen Bridged Systems. In *Comprehensive Coordination Chemsitry II: From the biology to nantechnology*; 2nd ed.; McCleverty, J. A.; Meyer, T. J., Ed; Elsevier: Oxford, 2004, 126−174.

(22) Berdiell, I. C.; Hochdörffer, T.; Desplanches, C.; Kulmaczewski, R.; Shahid, N.; Wolny, J. A.; Warriner, S. L.; Cespedes, O.; Schünemann, V.; Chastanet, G.; Halcrow, M. A. Supramolecular Iron Metallocubanes Exhibiting Site-Selective Thermal and Light-Induced Spin-Crossover. *J. Am. Chem. Soc.* **2019**, *141*, 18759−18770.

(23) Struch, N.; Bannwarth, C.; Ronson, T. K.; Lorenz, Y.; Mienert, B.; Wagner, N.; Engeser, M.; Bill, E.; Puttreddy, R.; Rissanen, K.; Beck, J.; Grimme, S.; Nitschke, J. R.; Lützen, A. An Octanuclear Metallosupramolecular Cage Designed To Exhibit Spin-Crossover Behavior. *Angew. Chem., Int. Ed.* **2017**, *56*, 4930−4935.

(24) Strohalm, M.; Hassman, M.; Košata, B.; Kodíček, M. MMass Data Miner: An Open Source Alternative for Mass Spectrometric Data Analysis. *Rapid Commun. Mass Spectrom.* **2008**, *22*, 905−908.

(25) Strohalm, M.; Kavan, D.; Novák, P.; Volný, M.; Havlíček, V. MMass 3: A Cross-Platform Software Environment for Precise Analysis of Mass Spectrometric Data. *Anal. Chem.* **2010**, *82*, 4648−4651.

(26) Niedermeyer, T. H. J.; Strohalm, M. MMass as a Software Tool for the Annotation of Cyclic Peptide Tandem Mass Spectra. *PLoS One* **2012**, *7*, e44913−e44913.

(27) *SAINT V6.22*; Bruker AXS Inc.: Madison, WI, USA, 2000.

(28) *SADABS V2.05*; Bruker AXS Inc.: Madison, WI, USA, 2001.

(29) Sheldrick, G. M. SHELXT - Integrated Space-Group and Crystal-Structure Determination. *Acta Crystallogr., Sect. A: Found. Adv.* **2015**, *71*, 3−8.

(30) Sheldrick, G. M. Crystal Structure Refinement with SHELXL. *Acta Crystallogr., Sect. C: Struct. Chem.* **2015**, *71*, 3−8.
(31) Blatov, V.; Shevchenko, A. ToposPro, Program Package for Multipurpose Crystallochemical Analysis. In *ToposPro VS.0, program package for multipurpose crystallochemical analysis*; 2014.
(32) Van Der Sluis, P. V.; Spek, A. L. BYPASS: An Effective Method for the Refinement of Crystal Structures Containing Disordered Solvent Regions. *Acta Crystallogr., Sect. A: Found. Crystallogr.* **1990**, *46*, 194−201.
(33) Spek, A. L. PLATON SQUEEZE: A Tool for the Calculation of the Disordered Solvent Contribution to the Calculated Structure Factors. *Acta Crystallogr. Sect. C Struct. Chem.* **2015**, *71*, 9−18.
(34) Brand, R. A. Improving the Validity of Hyperfine Field Distributions from Magnetic Alloys: Part I: Unpolarized source. *Nucl. Instrum. Methods Phys. Res., Sect. B* **1987**, *28*, 398−416.
(35) Bain, G. A.; Berry, J. F. Diamagnetic Corrections and Pascal's Constants. *J. Chem. Educ.* **2008**, *85*, 532−536.
(36) Chilton, N. F.; Anderson, R. P.; Turner, L. D.; Soncini, A.; Murray, K. S. PHI : A Powerful New Program for the Analysis of Anisotropic Monomeric and Exchange-Coupled Polynuclear *d*- and *f*-Block Complexes. *J. Comput. Chem.* **2013**, *34*, 1164−1175.
(37) Steckel, A.; Schlosser, G. An Organic Chemist's Guide to Electrospray Mass Spectrometric Structure Elucidation. *Molecules* **2019**, *24*, 611.
(38) McIndoe, J. S.; Vikse, K. L. Assigning the ESI Mass Spectra of Organometallic and Coordination Compounds. *J. Mass Spectrom.* **2019**, *54*, 466−479.
(39) Llunell, M.; Casanova, D.; Cirera, J.; Alemany, P.; Alvarez, S. *SHAPE V2.1*. SHAPE V2.1, Departament de Química Física, Departament de Química Inorgènica, and Institut de Química Teòrica i Computacional, Universitat de Barcelona: Barcelona, España, 2013.
(40) Angaridis, P.; Kampf, J. W.; Pecoraro, V. L. Multinuclear Fe(III) Complexes with Polydentate Ligands of the Family of Dicarboxyimidazoles: Nuclearity- and Topology-Controlled Syntheses and Magneto-Structural Correlations. *Inorg. Chem.* **2005**, *44*, 3626−3635.
(41) Sunatsuki, Y.; Ohta, H.; Kojima, M.; Ikuta, Y.; Goto, Y.; Matsumoto, N.; Iijima, S.; Akashi, H.; Kaizaki, S.; Dahan, F.; Tuchagues, J.-P. Supramolecular Spin-Crossover Iron Complexes Based on Imidazole-Imidazolate Hydrogen Bonds. *Inorg. Chem.* **2004**, *43*, 4154−4171.
(42) Liu, Y.; Kravtsov, V.; Walsh, R. D.; Poddar, P.; Srikanth, H.; Eddaoudi, M. Directed Assembly of Metal−Organic Cubes from Deliberately Predesigned Molecular Building Blocks. *Chem. Commun.* **2004**, *299*, 2806−2807.
(43) Xu, Q.; Zou, R.-Q.; Zhong, R.-Q.; Kachi-Terajima, C.; Takamizawa, S. Cubic Metal−Organic Polyhedrons of Nickel(II) Imidazoledicarboxylate Depositing Protons or Alkali Metal Ions. *Cryst. Growth Des.* **2008**, *8*, 2458−2463.
(44) Cheng, A.-L.; Liu, N.; Zhang, J.-Y.; Gao, E.-Q. Assembling the Cage-Based Metal−Organic Network from a Cubic Metalloligand. *Inorg. Chem.* **2007**, *46*, 1034−1035.
(45) Zou, R.-Q.; Sakurai, H.; Xu, Q. Preparation, Adsorption Properties, and Catalytic Activity of 3D Porous Metal−Organic Frameworks Composed of Cubic Building Blocks and Alkali-Metal Ions. *Angew. Chem., Int. Ed.* **2006**, *45*, 2542−2546.
(46) Alkordi, M. H.; Brant, J. A.; Wojtas, L.; Kravtsov, V. C.; Cairns, A. J.; Eddaoudi, M. Zeolite-like Metal- Organic Frameworks (ZMOFs) Based on the Directed Assembly of Finite Metal- Organic Cubes (MOCs). *J. Am. Chem. Soc.* **2009**, *131*, 17753−17755.
(47) Zhai, Q.-G.; Mao, C.; Zhao, X.; Lin, Q.; Bu, F.; Chen, X.; Bu, X.; Feng, P. Cooperative Crystallization of Heterometallic Indium-Chromium Metal-Organic Polyhedra and Their Fast Proton Conductivity. *Angew. Chem., Int. Ed.* **2015**, *54*, 7886−7890.
(48) Yamashita, T.; Hayes, P. Analysis of XPS Spectra of Fe^{2+} and Fe^{3+} Ions in Oxide Materials. *Appl. Surf. Sci.* **2008**, *254*, 2441−2449.
(49) Monti, M.; Santos, B.; Mascaraque, A.; de la Fuente, O. R.; Niño, M. A.; Menteş, T. O.; Locatelli, A.; McCarty, K. F.; Marco, J. F.; de la Figuera, J. Oxidation Pathways in Bicomponent Ultrathin Iron Oxide Films. *J. Phys. Chem. C* **2012**, *116*, 11539.
(50) Carrasco, E.; Oujja, M.; Sanz, M.; Marco, J. F.; Castillejo, M. X-Ray and Ion Irradiation Effects on Azurite, Malachite and Alizarin Pictorial Models. *Microchem. J.* **2018**, *137*, 381−391.
(51) Silva, K.; Marco, J. F.; Yañez, C. Covalent Immobilization of Amino-β-cyclodextrins on Glassy Carbon Electrode in Aqueous Media. *J. Electrochem. Soc.* **2019**, *166*, G75−G81.
(52) Haque, M. A.; Paliwal, L. J. Synthesis, Spectral Characterization and Thermal Aspects of Coordination Polymers of Some Transition Metal Ions with Adipoyl Bis(Isonicotinoylhydrazone). *J. Mol. Struct.* **2017**, *1134*, 278−291.
(53) Peng, H.; Chen, Z.; Tong, L.; Yu, X.; Ran, C.; Liu, Z. Thermochemical Hole Burning on a Triethylammonium Bis-7,7,8,8-Tetracyanoquinodimethane Charge-Transfer Complex Using Single-Walled Carbon Nanotube Scanning Tunneling Microscopy Tips. *J. Phys. Chem. B* **2005**, *109*, 3526−3530.
(54) Shi, S.-Y.; Chen, L.-Y.; Li, Y.; He, L.-H.; Zhang, J.; Cui, X.-B. Three New Hybrid Compounds Constructed from $\{PSb_2Mo_{12}O_{40}\}$ Polyoxoanions, TMMC or Organic Amines. *Inorg. Chem. Commun.* **2019**, *99*, 149−155.
(55) Guseva, G. B.; Ksenofontov, A. A.; Antina, E. V.; Barannikov, V. P.; Vyugin, A. I. Crystal Solvates of $Zinc^{(II)}$ Bis(Dipyrrinates) with Triethylamine: Composition, Stability and Spectral-Luminescent Properties. *J. Coord. Chem.* **2016**, *69*, 901−914.
(56) Sundaresan, S.; Kühne, I. A.; Kelly, C. T.; Barker, A.; Salley, D.; Müller-bunz, H.; Powell, A. K.; Morgan, G. G. Anion Influence on Spin State in Two Novel Fe(III) Compounds: $[Fe(5F\text{-}Sal_2333)]X$. *Crystals* **2019**, *9*, 19.
(57) Nihei, M.; Shiga, T.; Maeda, Y.; Oshio, H. Spin Crossover Iron(III) Complexes. *Coord. Chem. Rev.* **2007**, *251*, 2606−2621.
(58) Lescouëzec, R.; Vaissermann, J.; Lloret, F.; Julve, M.; Verdaguer, M. Ferromagnetic Coupling between Low- and High-Spin Iron(III) Ions in the Tetranuclear Complex *fac*-$\{[Fe^{III}\{HB(Pz)_3\}(CN)_2(\mu\text{-}CN)]_3Fe^{III}(H_2O)_3\}\cdot 6H_2O$ ($[HB(Pz)_3]^-$= Hydrotris(1-Pyrazolyl)-Borate). *Inorg. Chem.* **2002**, *41*, 5943−5945.
(59) Hoy, G. R. Relaxation Phenomena for Chemists. In *Mössbauer Spectroscopy Applied to Inorganic Chemistry*; Long, G. J. Ed.; Springer: Boston, MA, 1984; pp 195−226, DOI: 10.1007/978-1-4899-0462-1_8.
(60) Goura, J.; Bag, P.; Mereacre, V.; Powell, A. K.; Chandrasekhar, V. Molecular Iron(III) Phosphonates: Synthesis, Structure, Magnetism, and Mössbauer Studies. *Inorg. Chem.* **2014**, *53*, 8147−8154.
(61) Prodius, D.; Mereacre, V.; Singh, P.; Lan, Y.; Mameri, S.; Johnson, D. D.; Wernsdorfer, W.; Anson, C. E.; Powell, A. K. Influence of Lanthanides on Spin-Relaxation and Spin-Structure in a Family of Fe_7Ln_4 Single Molecule Magnets. *J. Mater. Chem. C* **2018**, *6*, 2862−2872.

https://dx.doi.org/10.1021/acsomega.0c02420
ACS Omega 2020, 5, 22238−22247